Journal of Materials Chemistry C

ROYAL SOCIETY OF CHEMISTRY

PAPER

View Article Online
View Journal | View Issue

Check for updates

Cite this: J. Mater. Chem. C, 2021, 9, 2455

Reversible data encryption–decryption using a pH stimuli-responsive hydrogel†

Hongjing Wen,[ab] Xianzhi Zeng,[b] Xiaoxuan Xu,[a] Wanyi Li,[b] Fei Xie,[b] Zhong Xiong,[c] Shichao Song,[b] Bin Wang,*[a] Xiangping Li[b] and Yaoyu Cao*[b]

Received 26th November 2020,
Accepted 6th January 2021

DOI: 10.1039/d0tc05578f

rsc.li/materials-c

In this work, based on a pH-responsive hydrogel, we report on a reversible data encryption–decryption technique in which the pH channel is employed for data manipulation. Upon alkali or acid stimulation, the hydrogel exhibits a network expansion or shrinkage in response to the pH variations. In particular, pre-doping the hydrogel with silver ions, we demonstrate that data input can be encoded in the hydrogel platform through the direct writing and patterning of silver nanodots. By this means, the scattering signals from the patterned nanodot pixels are converted to the binarized data. Meanwhile, we show the threshold behaviour of the hydrogel system in which dynamic switching of the encoded plasmonic pattern to the optically resolvable/irresolvable state is viable only at finite pH values. By delicately matching pixel spacings of the encoded pattern and the diffraction limit of the deciphering microscopic system, reversible sub-diffraction limit data encryption is achieved by selectively imposing acid and alkali stimulations. The suggested strategy offers a potential solution for optical storage, multiplexed data manipulation, and optical data security.

Introduction

With the development of optical storage technology, there has been an increasing demand of protecting data from intentional or unintentional leakage.[1,2] To date, several optical data encryption techniques have been developed and their applications in document security,[3–5] data storage,[6–8] and anti-counterfeiting[9–11] have been found. However, it is still a challenge to explore new encoding channels for data encryption and efforts have been made to diversify the encoding–decoding approaches to guarantee the confidentiality of the classified data.

To this end, recently, stimuli-responsive materials have received tremendous attention and have been considered as promising media for data security applications.[12–19] Exploiting the unique reactive properties of these smart materials, various data encryption platforms have been designed employing carbon dot composites,[20] mechanochromic hydrogels,[21] luminescent hydrogels,[22] *etc.* Among various intelligent reactive materials, pH-responsive hydrogels could be a suitable platform providing pH sensitivity for data manipulation and are operable in liquid environments,[23–27] yet little research has addressed their potential for data security applications.

Here, we demonstrate that using a pH-responsive composite hydrogel the reversible data encryption–decryption could be achieved. In this study, an alkaline-expanding hydrogel was prepared based on the acrylic acid (AAc) monomer and poly(ethylene glycol) diacrylate (PEGDA) crosslinker.[28] We show that the AAc/PEGDA hydrogel can reversibly expand/shrink in response to specific alkaline/acidic stimulations without obvious fatigue. Besides, dynamic threshold behaviour of the pH-responsive hydrogel that both expansion and shrinkage can be triggered only at correct alkali or acid values. Pre-doped with the diamine silver complex, the hydrogel matrix was used as a dynamic platform. Upon irradiation of a femtosecond laser beam, $[Ag(NH_3)_2]^+$ complex ions near the tight focus can gain energy through the two-photon absorption (TPA) process and dissociate to form neutral Ag nanodots attached to the gel network.[29] Remarkably, compared to the photoluminescent dyes employed in common strategies, Ag nanodots are free of the adverse photobleaching effect and exhibit intense scattering from their surface plasmon effect like other noble metals,[30] making them compelling candidates for optical data storage and reversible data encryption. In this work, through programmatically positioning the focused

[a] The Key Laboratory of Weak-Light Nonlinear Photonics, Ministry of Education, School of Physics, Nankai University, Tianjin 300071, China. E-mail: wb@nankai.edu.cn
[b] Guangdong Provincial Key Laboratory of Optical Fiber Sensing and Communications, Institute of Photonics Technology, Jinan University, Guangzhou 511443, P. R. China. E-mail: yaoyucao@jnu.edu.cn
[c] College of Chemistry and Chemical Engineering and Institute of Marine Biobased Materials, Shandong Collaborative Innovation Center of Marine Biobased Fibers and Ecological Textiles, State Key Laboratory of Bio-fibers and Ecotextiles, Qingdao University, Qingdao 266071, China

† Electronic supplementary information (ESI) available. See DOI: 10.1039/d0tc05578f

laser beam, an arbitrary plasmonic pattern, which was composed of discrete silver nanodots, can be generated in the expanded platform. Considering each nanodot as a recording pixel resembling state "1", the input nanodot pattern with the scattering signals from the inscribed plasmonic structures converted to binarized data. During the inscription process, pixel spacings were precisely controlled to be close to the resolving limit of the decoding microscopic system. We demonstrate that the shrinkage of the pre-expanded platform could occur below the acid threshold, driving the pixel spacings to the sub-diffraction region where the patterned data were obfuscated by the diffraction barrier. And the encrypted data could only be resolved again when the gel platform was re-treated at correct alkali value.

Results and discussion

The basic principle of the suggested pH-responsive cryptography is illustrated in Fig. 1. The prepared AAc/PEGDA composite hydrogel could accordingly expand/shrink following specific alkaline/acidic stimuli, giving rise to a geometrical scaling of the gel network. Meanwhile, through sequentially exposing to ultrafast laser pulses, silver ions in the gel platform could gain energy from the photon flux and undergo the well-known TPA process, after which the excited ions could capture electrons from donors and be reduced to form elemental silver. By this means, binarized raw data could be stored in scattering nanostructures,

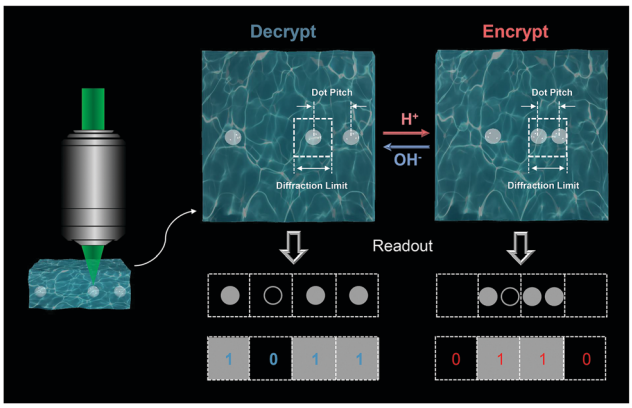

Fig. 1 Basic principle of the suggested pH-responsive cryptography. Data encryption can be achieved *via* treating the hydrogel platform with specific pH stimuli. Expansion or shrinkage of the platform can be accordingly triggered upon alkaline or acidic stimulation. Then, the repulsive or attractive force will induce the change of both the hydrogel platform and the pre-inscribed recording nanostructure geometrical scaling. In this way, through carefully matching the dot pixels in the recording structure to the resolving limit of the optical receiver, the pixel spacing can be switched in or out of the sub-diffraction regime, where the original message is distorted due to the diffraction disturbance from the adjacent pixels. For simplicity, the lateral resolving limit (resolution) of the receiving optical microscope is represented as the rectangular dashed cells. Spacings of the recording pixels at the alkaline-active expansion state are initially controlled to be slightly larger than the resolving limit; if specific acid stimuli are implemented, owing to the shrinkage effect of the hydrogel, there could be more than one pixel in a cell, and the signal from this cell therefore must be distorted.

and the discrete silver dot pixels played the role of recording pixels representing the state "1" while the vacancy represented the state "0". As depicted in Fig. 1, binary code "1011" in the form of a 1D silver dot sequence can be initially input in the expanded gel platform, that is, the platform is treated at a particular alkaline pH value. Upon exposure to external pH stimuli, the scaling effect of the platform can effectively interfere with the readout of the scattering signals from the embedded nanodot pixels. Specifically, spacings of the adjacent dot pixels were set to be slightly larger than the lateral resolving limit of the optical receiver, which for simplicity was represented as the unit cells of a dashed grid. On being treated with acid, collapse of the gel network would be activated driving the pixel spacings to the sub-diffraction region, which alternatively meant that there could be more than one pixel inside one single cell. As a result, even the dot sequence itself was not physically demolished or replaced, secured by the diffraction barrier, the original message stored in the sequence was obfuscated and the scattering signals extracted by the receiver were distorted to be the wrong message, which was "0110" for the case in Fig. 1. Input data could be correctly decrypted and readout only when the platform is re-treated with the suitable alkaline pH value.

As an appealing tunable platform for hosting the production of silver structures, the acrylic acid (AAc)/poly(ethylene glycol) diacrylate (PEGDA) composite hydrogel offers homogenous environment for the reactants to stably photoproduce silver structures in the interior of the gel. The pH-responsive behavior of the AAc/PEGDA composite hydrogel originates from the reversible deprotonation/protonation of the rich carboxyl groups of AAc in alkaline/acid environments.[31] Deprotonated by the hydroxide ions, increasing density of COO^- within the hydrogel network could induce the phase transition due to electrostatic repulsion, driving the hydrogel to expand. Reversely, on protonated by acid stimulation, the decrease in the charge density of the network cannot support the network expansion leading to hydrogel shrinkage. The pH-responsive hydrogel solution was first configured which was colorless and transparent as in Fig. 2a and then the hydrogel was formed by UV curing with a porous structure. The ultraviolet-visible (UV-vis) absorption spectrum of the hydrogel is shown in Fig. S1 (ESI†). And the swelling ratio, defined by W_s/W_d, of the pH-responsive hydrogel in deionized water shown in Fig. S2 (ESI†) which reflected the hydrogel reaches swelling equilibrium in less than two minutes, where W_s and W_d are the wet weight and dry weight of the hydrogel, respectively.[28] To testify the pH-responsive scaling behavior of the AAc/PEGDA composite hydrogel, expansion tests of fresh AAc/PEGDA hydrogel discs, which were preserved in deionized water with 6 mm original sizes, were conducted by soaking the sample discs in aqueous solutions at different pH values. As demonstrated in Fig. 2b, sample gel discs treated at pH values ascending from 1.5 to 10 remained almost unchanged with a scaling factor of exactly 1.0 (correspond to d = 6 mm). However, for those treated at higher pH values, obvious deformations with scaling factors larger than 1 were observed, indicating the expansion of the hydrogel network. The threshold phenomena could be attributed to the electrostatic effect endowed by ionization

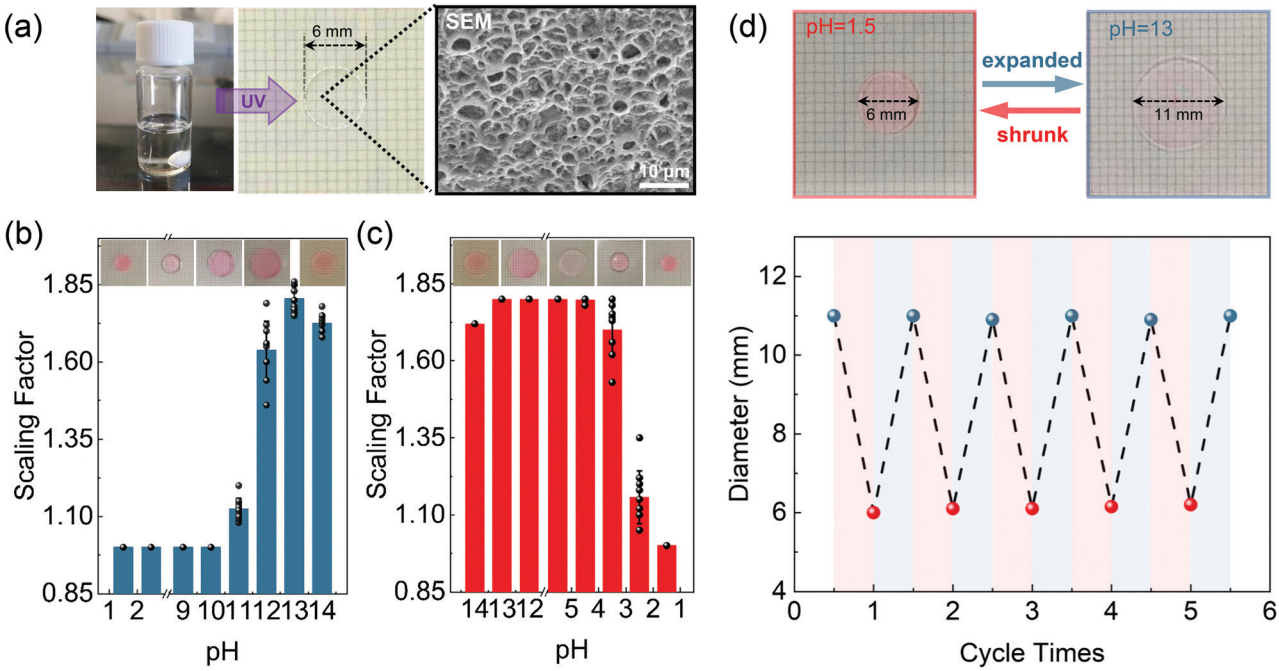

Fig. 2 Characterization of the pH-responsive hydrogel. (a) Left to right: Photograph of the AAc/PEGDA pre-gel solution (left), sliced hydrogel disc (middle), and SEM image of the internal gel network (right). (b) and (c) Scaling factors and corresponding photos of the hydrogel obtained at different pH values, threshold behavior that expansion and shrinkage only occur at pH exceeding particular values can be observed, the acidic and alkaline thresholds appear at 4.5 and 10 and the maximum/minimum scaling factor can be found at pH 13 and pH 1.5 respectively. (d) Repeatability test of pH-responsive scaling of the hydrogel (tinted by Rhodamine 6G). The upper pictures show the size changes of the hydrogel disc responding to the acidic (pH = 1.5) and alkaline (pH = 13) environment, the figure below shows the changes of gel disc diameter during five pH variation cycles.

of the carboxyl group of the AAc monomer. At pH values higher than 10, the electronic donors, *i.e.*, the hydroxide anions, in the environmental fluid are sufficient to break the proton balance, providing dominant repulsion force to activate the expansion of the gel network. And a maximum scaling factor was found to be 1.8 at pH 13 (correspond to d = 11 mm), and the pH-responsive hydrogel reached the fully-expanded state when the carboxyl groups of the AAc components were almost consumed and ionized. Meanwhile, it should be noted that a decreased scaling factor was observed at pH 14, which can be ascribed to the excessive hydroxide in the medium. It was the repulsion between the ions inside and outside the network that suppresses the further expansion of the gel network.

The shrinkage effect was next studied by reversely protonating the alkaline liquids (pH = 13). Similarly, the expanded samples remained at nearly the same size with a scaling factor of 1.8 until reaching an acidic threshold at pH 4.5, and returned to the original size at pH 1.5 (Fig. 2c). In this case, the hydroxide ions in the hydrogel were completely consumed, and the weakened repulsive force could no longer support the extension of the network, therefore causing the collapse of the gel platform. Furthermore, the reversibility of the expanding/shrinking effect of the AAc/PEGDA hydrogel was investigated by repetitively soaking one gel disc in NaOH solution (pH = 13) and HNO_3 solution (pH = 1.5) for 5 cycles. As demonstrated in Fig. 2d, the diameter of the sample disc consistently varies between the expanded state (11 mm) and shrunk state (6 mm) without obvious fatigue. The excellent repeatability further confirms that the synthesized hydrogel is competent to serve as a platform for dynamic pH modulation.

As described in the context, the 1D dot sequence or 2D dot array can be first inscribed in the expanded hydrogel platform *via* femtosecond direct laser writing (DLW) of silver dots, through which raw data are stored in the scattering nanostructures before the encryption process. Besides, it is worth mentioning that the inscription procedure will not give rise to any undesired deformation of the gel platform. As shown by the photographs in Fig. 3a, neither shape nor size alternation of the gel disc (tinted with rhodamine 6G) was observed before and after the inscription of the scattering pixels but only an enhancement of the overall scattering intensity. The TEM image of one silver dot in the pH-responsive hydrogel is shown in Fig. S3(ESI†). Moreover, in order to investigate the uniformity of the scattering signals from the written structures, a 2 × 5 silver dot array was recorded in the hydrogel with a laser power of 1 mW and an exposure time of 80 ms. Dark-field images and the corresponding scattering intensities extracted along the dashed lines exhibit that the intensity fluctuations are less than 10%, which further confirms the favorable homogeneity of the written silver array (Fig. 3b). And the size characteristics of the silver dot array with different writing powers (0.1–1.0 mW) can be seen in Fig. S4 (ESI†).

Furthermore, influences of pH stimulus on the dot pixels in the gel platform were investigated. Typically, a 4 × 4 silver dot array was first fabricated in the expanded gel disc (treated at pH = 13), after which the liquid bath was successively acidified

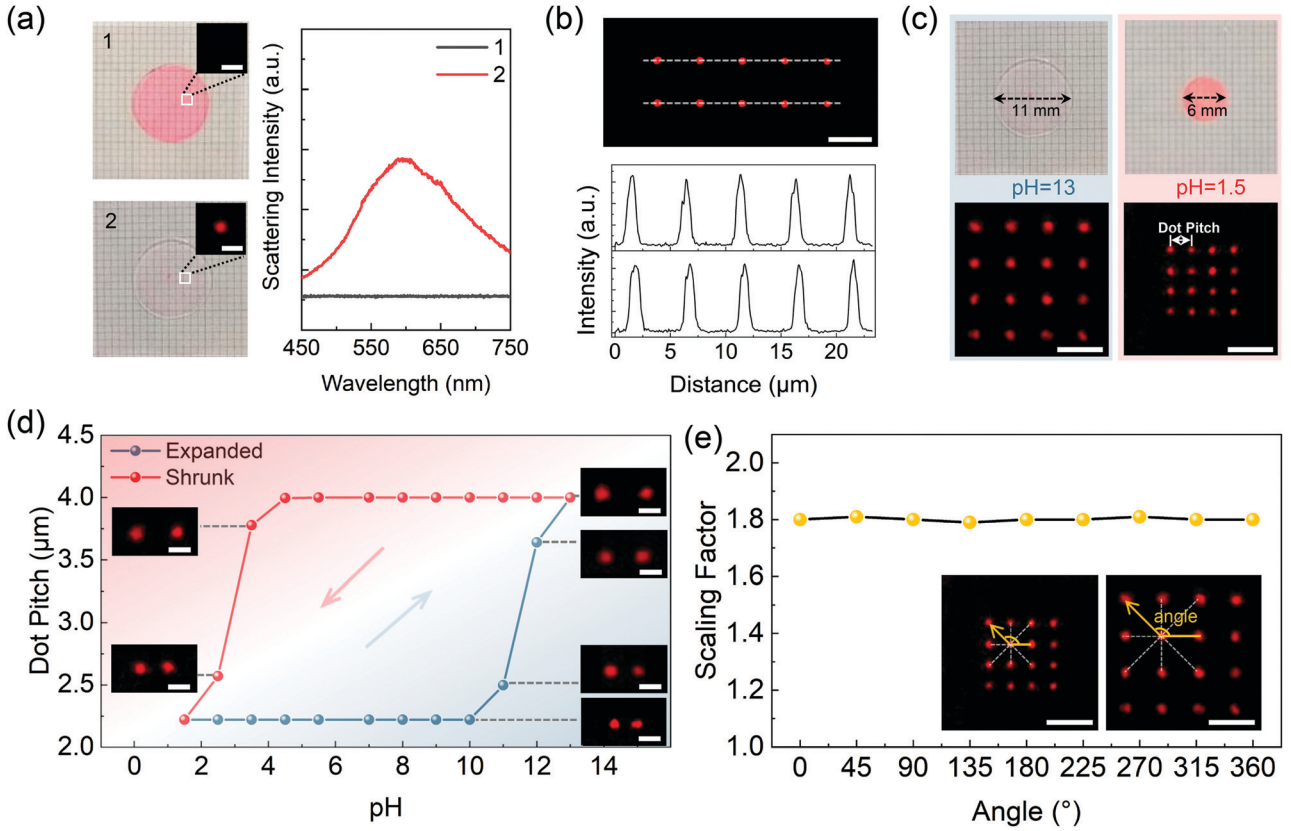

Fig. 3 Dynamics of the recording pixels in the hydrogel platform. (a) Left: Comparison of the hydrogel discs (d = 6 mm) with (disc 1) and without (disc 2) data inscription. Both discs are tinted by Rhodamine 6G. Insets: Dark-field images of the single pixel. Right: Scattering spectra measured in the white box areas of discs 1 and 2. (b) The dark-field scattering image of the 2 × 5 silver dot lattice. And the corresponding scattering intensities of the two white marked areas are depicted nether the dark-field scattering image, which shows reasonable uniformity of scattering intensity. (c) Influences of the pH-responsive scaling effect on the inscribed 4 × 4 scattering array inside the gel disc platform. When treated at pH 13, an overall expansion is imposed on the gel network causing the stretch of the array. However, when treated at pH 1.5, the gel disc returns as the original size with a decreased dot spacing. (d) Variation of dot spacings of the two silver dots in one pH-varying cycle. Dot spacings of the array remain unchanged until reaching pH 10 for the alkalizing panel and 4.5 for the acidizing panel. The spacing ratio of the dot spacing at pH 13 to that at pH 1.5 equals the scaling factor calculated at pH 13, indicating the overall effect of the platform scaling. The insets depict the dark-field images of the two silver dots. (e) Homogeneity test of the platform scaling along omnidirections. Dot spacings between the marked dot and the eight adjacent pixels, which correspond to the angles from 0° to 360°, are measured. The insets show the dark-field images of the array at the shrunk state and expanded state. Scale bars in (a) and (d) are all 2 μm. Scale bars in (b), (c) and (e) are all 5 μm. All silver dots are written at an average power of 1 mW with an exposure time of 80 ms.

and then re-alkalized through drop casting HNO_3 solution and NaOH solution until a pH-varying cycle was completed. Meanwhile, after the equilibrium state was achieved, the scattering array was imaged at each pH step to record the changes of the pixel spacings. Photographs of the expanded/shrunk gel disc as well as the corresponding dark-field images of the scattering array are presented in Fig. 3c. Variations of pixel spacings during one pH-varying cycle are demonstrated in Fig. 3d, where the two threshold pH values that activate the network expansion and shrinkage of the platform appear at 4.5 and 10. The broad pH band, in which the gel platform remains as its former state, has ensured the limited response to the pH stimuli. Hence, except for the two threshold values, the distorted scattering signals could not be corrected with the invalid pH stimulus, thereby realizing optical encryption of the input message. Furthermore, it was found that the spacing ratio of the dot spacing between pH 13 and pH 1.5 equals 1.8, which coincided with the scaling factor of the platform treated at pH 13. The well-matched result revealed the synchronic variation of the platform as well as the pixel spacing of the inscribed array and the defined scaling factor also applied to the change of dot spacing. In addition, homogeneity during the scaling of the hydrogel platform was also verified, as exhibited in Fig. 3e, dot spacings between the marked pixel and its eight adjacent dots at expanded and shrunk states were measured at the equilibrium state (inset image). Substituting the measured values into eqn (1), the scaling factors of the eight directions were calculated, as presented, a negligible standard deviation as small as 0.6% was obtained, indicating the extraordinary uniformity during the platform scaling.

It is well known that the resolution of an imaging system is fixed with a determined point spread function (PSF), and that the angular resolving ability could be described using the Rayleigh criterion, which is given by 0.61λ/NA (where λ is the wavelength of the incident light and NA is the numerical aperture of the objective lens). Due to the diffraction nature

of light, the distance of two objects closer than the Rayleigh criterion could hardly be distinguished by the optical system in use. In our strategy, aided with the high-precision DLW technique, spacings of the recording pixels were controlled to be slightly larger than the Rayleigh criterion of the receiving optical microscope so that the shrinkage of the pre-expanded platform would drive the pixel spacings to the sub-diffraction regime. Consequently, crosstalk between the individual PSFs would distort the original scattering signals, and one would be incapable of deciphering the attained scattering signals into correct messages.

As a proof-of-concept demonstration, a customized silver nanodot array has been designed and is illustrated in Fig. 4a. The array was composed of silver nanodots with two different dot spacings, which were denoted by l_1 (l_1 = 500 nm) and l_2 (l_2 = 250 nm), respectively. The dot elements with spacings of l_1 were employed as the recording pixels and could be imaged as a quasi-analog pattern due to the sub-diffraction pixel spacing, while the ones with spacings of l_2 played the role of diffraction noise sources. Initially, an Arabic number "2" was input in the expanded platform (pH = 13) by positioning the ultrafast laser beam along a predetermined trajectory, as shown in Fig. 4a (top). A dark-field microscope with a lateral resolution of about 393 nm was employed as the optical receiver (λ = 580 nm, NA = 0.9). To elucidate the influence of the pH-responsive scaling of the platform on the input message, a line grid whose unit cells refer to the lateral resolving limit of the receiver is illustrated and demonstrated in the middle of Fig. 4a. The cells filled with recording dots are the pixels representing code "1" while the hollow ones mean code "0". The corresponding coding diagram is exhibited in the bottom figure of Fig. 4a.

At first, as demonstrated in Fig. 4a (middle), the density of the recording pixels was approximately two times higher than that of the noise pixels, and it was also higher than the diffraction limit of the dark-field microscope system. As discussed above, the message was supposed to be at the decrypted state, and noise pixels merely acted as the additive background noise. In this case, message "2" can be read out with a sufficient

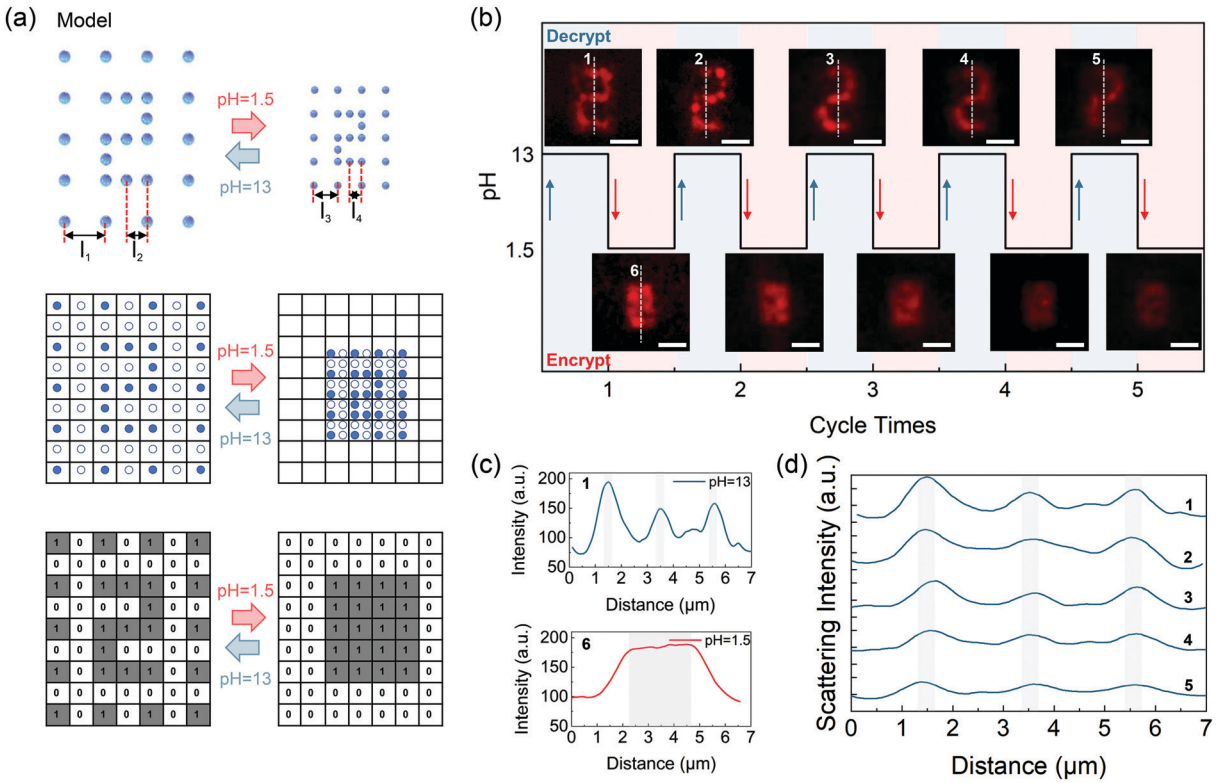

Fig. 4 Proof-of-concept experiment for optical data encryption and decryption. (a) Top: Designed scattering array where the dot elements possess two different spacings of l_1 (500 nm) and l_2 (250 nm) at the expansion state of pH 13 (lateral resolution of the receiving microscope is 393 nm, and the array is written with an average power of 0.1 mW and an exposure time of 80 ms). Dots with the sub-diffraction spacing l_2 are selected as the recording pixels providing effective scattering signals while the ones with l_1 are the additive noise sources ensuring confidentiality of the message during the acid-active encryption process. When treated at pH 1.5, driven by the shrinking effect of the platform, the dot spacings are replaced with $l_3 = l_1/1.8$, and $l_4 = l_2/1.8$, which are both in the sub-diffraction regime. Middle: Illustration of the relationship between the lateral resolution of the receiver and the dot spacings at expanded and shrunk states. Bottom: Corresponding coded diagrams of the scattering array, at the shrunk state, crosstalk between the scattering signals from the recording pixels and noise ones is introduced, interfering the readout of the original message. (b) Reproducibility test of pH-responsive information in the hydrogel. Dark-field images of the messages acquired by the receiver when the platform is at decrypted or encrypted states (scale bars: 2 μm). (c) Scattering intensity profiles measured along the dashed line 1 and dashed line 6 in (b), the three peaks mark the visual feature of the horizontal lines of message "2", disturbing signals from the noise pixels can blur the characterizing peaks thereby delivering a distinct message. (d) Scattering intensity profiles measured along the dashed lines 1–5 in (b).

signal-to-noise ratio (SNR). As the liquid environment acidized at pH 1.5, an overall shrinkage of the scattering array led to the collapse of the gel network. At this time, l_1 and l_2 were replaced by l_3 and l_4, which were both closer than the resolving limit of the microscope and could be calculated by simply dividing l_1 and l_2 with the scaling factor. Meanwhile, owing to the shrinkage effect of the platform, the noise pixels were then close enough to induce conspicuous crosstalk between the diffraction noise and the effective signals, which means that the original message is secured by the additive noises. Thus, what the receiver acquired was a fuzzy image with message "2" being optically encrypted. Reversely, when the environmental liquid was re-alkalized at the decrypting pH value, the sub-diffraction spacing l_3 was stretched back to l_1 following the expansion of the platform, eliminating the crosstalk between the scattering signals from the recording and noise pixels and guaranteeing a high SNR for data readout on the receiver side.

Fig. 4b confirms the encryption principle proposed in Fig. 4a and shows the reproducibility of information "2" that can be read repeatedly in five circles. The visual feature of Arabic "2" can be ascribed to the three horizontal-line structures in the pattern. Therefore, whether these three horizontal line structures are spectrally recognizable or not can be used as a criterion for distinguishing the scattering pattern. Fig. 4c demonstrates the cross-sectional scattering intensity profiles plotted along the white dotted line 1 and line 6 in the dark-field images of Fig. 4b. The line structures were considered as recognizable if the valley-to-peak ratios of the characterizing peaks in the scattering spectra were less than 73.5%, which can be judged to distinguish peaks effectively according to the Rayleigh criterion. At pH 13, three well-separated peaks can be observed with the valley-to-peak ratios of the central peak being 30% and 39% respectively (background scattering intensity was measured to be about 70), indicating that the pattern was at the resolvable state. At acidic pH value (pH 1.5), however, the collapsed network caused the shrinkage of the entire dot array, by which the visual feature was erased due to the introduction of extra noise, leaving one broad band peak observed. Fig. 4d shows the cross-sectional scattering intensity profiles plotted along the white dotted lines 1–5 in the dark-field images of Fig. 4b. When stimulated at the suitable alkaline pH value, *i.e.*, pH 13, dot spacings of the noise pixels recovered to be further than the Rayleigh criterion, crosstalk between the noise and the three characterizing peaks were eliminated. Furthermore, spacings of the scattering peaks of the structural features of Arabic message "2" remained almost unchanged during five cycles. The valley-to-peak ratios of the central peak of line 5 are 51% and 44%, therefore the encoded message can still be readout without distortion after five cycles. However, it is true that as the repeating expanding–shrinking cycles increases the scattering peak intensity of silver structures decreases accompanied by a lowered signal-to-noise ratio of the information.

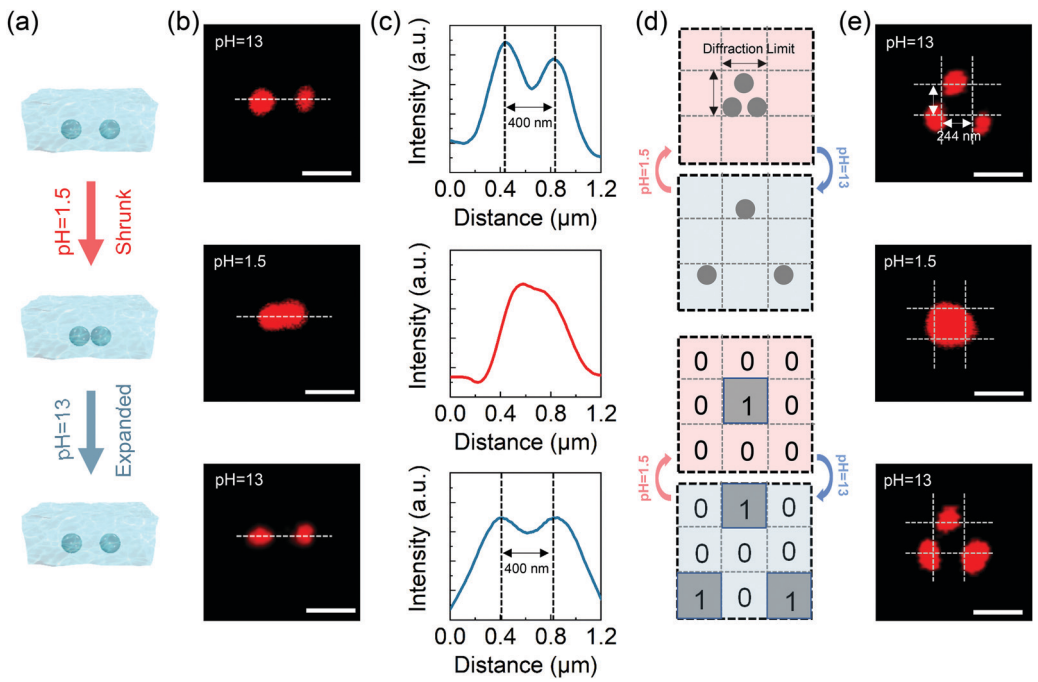

Fig. 5 Sub-diffraction limit feature of the reported strategy. (a) Schematic diagrams of variations of pixel spacing of the 1D bi-dot array in the expanded/shrunk hydrogel platform. (b) Received images of the bi-dot array (written at an average power of 0.1 mW with an exposure time of 80 ms) of the employed confocal microscope (lateral resolution: 244 nm). Left to right: Dynamic switch of the two dot pixels to resolvable (top), irresolvable (middle), and resolvable (bottom) states by protonating the liquid bath of the pre-expanded platform (pH 13) to pH 1.5 then deprotonating back to pH 13. (c) Intensity profiles of the scattering signals plotted along the dashed lines in (b). The two scattering peaks merge to be one entity while treating the platform at pH 1.5 but are then separated again at pH 13. Scale bars are all 400 nm. (d) Schematics of reversible data encryption of the 2D tri-dot array and the change of received message at the expansion/shrinkage state. (e) Received images of the tri-dot array in experiment. Scale bars are all 400 nm.

The intensity change is ascribed to the surface oxidation of the nanodot carriers by the atmospheric oxygen.

To highlight the sub-diffraction limit feature of our strategy, reversible encryption of 1D and 2D dot arrays is presented in Fig. 5 as intuitive examples. As shown in Fig. 5a, a bi-dot array storing code "11" was first inscribed in the pre-expanded platform and an encryption/decryption cycle was performed taking the encryption and decryption pH value to be 1.5 and 13. Pixel spacing was precisely set to be 400 nm before the implementation of acidic stimulation. Because the pixel spacing was larger than the diffraction limit, *i.e.*, lateral resolution, of the receiving microscope, which was 244 nm, the encoded message "11" can be optically read out by the confocal microscopy system. Then, when the pH value of the liquid bath was altered to be 1.5, the shrinkage of the gel body forced the dot spacing to narrow from 400 nm to 222 nm, which was closer than the diffraction limit of 244 nm. At this point, crosstalk between the PSFs of the pixels resulted in a blurred image, in which the extracted message became code "1". However, as the hydrogel was re-treated with the suitable alkali pH value, 13, the dot spacing recovered to be 400 nm reinforced by the expansion of the gel network, then the message "11" was optically reconstructed and could be correctly read out again (Fig. 5b). Changes of intensity profiles of the scattering nanodots are demonstrated in Fig. 5c, and the two peaks that characterize the coded pixels merged to be one single peak at pH 1.5 but could again be separated at pH 13.

For the 2D case, a tri-dot array recording a binary matrix was designed and, similar to the 1D case, initially inscribed in the pre-expanded platform, as illustrated in Fig. 5d. Again, dashed grids, whose side length marked the diffraction limit of the microscope (244 nm), were used to depict the interrelationship between the diffraction limit of the deciphering microscope and pixel spacings. Confocal scattering images received by the microscope system are demonstrated in Fig. 5e. The inter-pixel spacings were first accurately set to be the same as the diffraction limit. On stimulating at acid pH value (pH = 1.5), the three encoding pixels, which were (1, 2), (3, 1) and (3, 2) elements, were all pulled in the central grid, which meant that the inter-pixel spacings were closer than the diffraction limit. As a result, the extracted matrix was distorted leaving merely the (2, 2) element to be at "1" state (middle figure of Fig. 5e). But when the platform was re-treated at alkali pH value (pH = 13), expansion of the network drove the pixel spacings out of the sub-diffraction limit regime, a correct readout was restored with the encoding pixels relocated at their original sites, suggesting the fatigue-free feature of the reported sub-diffraction limit encryption strategy.

Conclusions

In conclusion, an AAc/PEGDA pH-responsive hydrogel was fabricated and used as the dynamic platform for optical data encryption. It was found that the hydrogel could expand/shrink in response to pH interference, while the threshold behavior in which pH-responsive scaling of the gel matrix can only be triggered at particular pH values was observed. Utilizing the threshold effect, an external pH stimulus was used as the encryption/decryption key to initiate shrinkage/expansion of the platform whereby spacings of the encoding pixels can be reversibly modulated in/out of the sub-diffraction regime. Through precisely matching the lateral resolution of the deciphering optical system and the scaling factor of the gel platform, a customized micropattern was designed with the input data discretely stored in the recording pixels. Furthermore, the sub-diffraction limit feature of the proposed strategy was also demonstrated. It was shown that dynamic switch of both the customized pattern and data matrices between the optically encrypted/decrypted states can be reversibly performed with no obvious signal distortion. Secured by the diffraction nature of light, the encrypted message can only be correctly read out when the platform was treated at the suitable pH value, which was 13 for the reported hydrogel. This facile and reproducible strategy offers a solution for optical data encryption in liquid environments and could potentially be applied in multidimensional data storage and security applications.

Experimental section

Materials

Acrylic acid (AAc) was purchased from Shanghai Macklin Biochemical Co., Ltd. Poly(ethylene glycol) diacrylate (PEGDA) was purchased from Aladdin. *n*-Decanoylsarcosine sodium (NDSS)[32] was acquired from Tokyo Chemical Industry. Azobisisobutyronitrile (AIBN) was supplied by Shanghai Macklin Biochemical Co., Ltd. Dimethyl sulfoxide (DMSO, ST038) was purchased from Beyotime. Sodium hydroxide (NaOH) and nitric acid (HNO_3, G.R.) were purchased from Sigma Aldrich. All chemical reagents were of analytical grade and used without further purification. Throughout this work, aqueous solutions were prepared using ultrapure water (Smart2Pure, ThermoFisher).

Preparation of the AAc/PEGDA composite hydrogel

The pH-responsive hydrogel was prepared with a two-step procedure, acrylic acid (0.7 g) as the monomer, PEGDA (0.3 g) as the crosslinker and the initiator AIBN (0.05 g) were first mixed with DMSO (1.0 g) and stirred for 20 minutes to form a homogeneous solution. The mixed pre-gel solution was then cured under UV irradiation (395 nm, 5 min) to form the gel network. Subsequently, the product was rinsed with deionized water to remove the residual DMSO. The AAc/PEGDA hydrogel was then dipped in fresh NDSS/diamine silver solution (C_{Ag^+}: 0.01 mol L^{-1}, C_{NDSS}: 0.01 mol L^{-1}) for 1 min to allow the silver ions to diffuse into the hydrogel network. The resulting composite hydrogel was sliced carefully into the thin disc for the following experiments.

Acid/alkali treatments

The sensitivity of the composite hydrogel to external pH stimuli was examined by immersing the gel discs into liquid baths at different pH values, which were prepared by diluting NaOH and HNO_3 aqueous solutions. Gel disc diameters were measured

after the equilibrium state was reached. Scaling factor r that quantifies the geometrical variation of the hydrogel was defined as follows:

$$r = \frac{d}{d_0} \quad (1)$$

where d_0 (6 mm) represents the gel disc original diameter in a fully water-filled state in deionized water and without the implementation of pH stimuli and d represents the gel disc diameter with the implementation of pH stimuli.

Data inscription

To store the input data in the AAc/PEGDA hydrogel, the expanded/shrunk gel discs were sealed between cleansed silica slides and cover slips. Then the samples were mounted on a three-dimensional piezostage (P-563.3CD, Physik Instrumente (PI) GmbH & Co. KG) which enabled translational and axial displacements of the sample. A 532 nm femtosecond laser beam (210 fs, 80 MHz) was employed for data inscription and tightly focused onto the sample through an oil-immersion objective (100×, NA = 1.4, Olympus). The focal spot size was estimated to be about 232 nm, according to the formula $D = 0.61 \times \lambda_{dlw}/NA$,[33] where λ_{dlw} is the laser wavelength of direct laser writing (DLW). Raw data were recorded in the gel platform *via* the sequential exposure of the platform to the ultrafast laser beam from site to site. A CCD camera (MER-132-43U3M-L, Daheng) that provided a magnified field of view was used to monitor the fabrication process.

Measurements and characterization

Internal morphology analysis of the composite hydrogel was conducted using a scanning electron microscope (SEM). Before observation, the hydrogel was freeze-dried to remove the moisture thoroughly and then sputtered with a thin gold coating. A confocal microscope was used to extract the scattering signals from the plasmonic pattern embedded in the gel platform. A continuous-wave laser (561 nm) was used for sample illumination. Operated at a fixed power of 200 μW, the incident laser beam was focused on the sample using an oil-immersion objective (100×, NA = 1.4), and backward scattering signals were collected using the same lens and detected using a photomultiplier tube (PMT) placed behind the confocal pinhole. The resolving limit (D_1) of the confocal imaging system was calculated to be 244 nm. And a dark-field microscope system, where a white light with a central wavelength of 580 nm as well as an objective of 0.9 NA (MPlanFLN, 100×/0.9 BD, Olympus) provided a resolving limit of 393 nm (D_2), was employed to decipher the signals from the customized pattern.

Author contributions

Y. C. conceived the project. B. W., Y. C. and X. L. supervised the project. H. W. and Y. C. designed all experiments. H. W. conducted the fabrication and characterization of the silver structures and the pH-responsive hydrogel. H. W., X. Z. and Y. C. prepared the manuscript, H. W. and Y. C. prepared the figures, and all authors participated in experiment data analysis and manuscript editing.

Conflicts of interest

There are no conflicts to declare.

Acknowledgements

This research was supported by the National Key R&D Program of China (YS2018YFB110012), the National Natural Science Foundation of China (NSFC) (Grant 61605061, 61875073, and 61675093), the Guangdong Provincial Innovation and Entrepreneurship Project (Grant 2016ZT06D081), the Guangdong Basic and Applied Basic Research Foundation (Grant No. 2019A1515110385), the Fundamental Research Funds for the Central Universities, the Science and Technology Support Program of Tianjin (Grant No. 15ZCZDGX00780), the National Key R&D Program of China (Grant No. 2016YFC0400709), and the Program for High-Level Entrepreneurial and Innovative Talents Introduction of Jiangsu Province (2019&2020).

References

1 M. Gu, X. Li and Y. Cao, *Light: Sci. Appl.*, 2014, **3**, e177–e177.
2 O. Matoba, T. Nomura, E. Perez-Cabre, M. S. Millan and B. Javidi, *Proc. IEEE*, 2009, **97**, 1128–1148.
3 J. M. Meruga, W. M. Cross, P. S. May, Q. Luu, G. A. Crawford and J. J. Kellar, *Nanotechnology*, 2012, **23**, 395201.
4 C. Lin, X. Shen and B. Li, *Opt. Express*, 2014, **22**, 20727–20739.
5 Z. Liu, Q. Guo, L. Xu, M. A. Ahmad and S. Liu, *Opt. Express*, 2010, **18**, 12033–12043.
6 H. H. Pham, I. Gourevich, J. K. Oh, J. E. Jonkman and E. Kumacheva, *Adv. Mater.*, 2004, **16**, 516–520.
7 Y. Chen, X. Yang and J. Gao, *Light: Sci. Appl.*, 2019, **8**, 1–9.
8 X. Tan, O. Matoba, T. Shimura, K. Kuroda and B. Javidi, *Appl. Opt.*, 2000, **39**, 6689–6694.
9 T. Sun, B. Xu, B. Chen, X. Chen, M. Li, P. Shi and F. Wang, *Nanoscale*, 2017, **9**, 2701–2705.
10 Y. Heo, H. Kang, J. S. Lee, Y. K. Oh and S. H. Kim, *Small*, 2016, **12**, 3819–3826.
11 Z. Long, Y. Wen, J. Zhou, J. Qiu, H. Wu, X. Xu, X. Yu, D. Zhou, J. Yu and Q. Wang, *Adv. Opt. Mater.*, 2019, **7**, 1900006.
12 J. Hai, T. Li, J. Su, W. Liu, Y. Ju, B. Wang and Y. Hou, *Angew. Chem., Int. Ed.*, 2018, **57**, 6786–6790.
13 Y. Su, S. Z. F. Phua, Y. Li, X. Zhou, D. Jana, G. Liu, W. Q. Lim, W. K. Ong, C. Yang and Y. Zhao, *Sci. Adv.*, 2018, **4**, eaas9732.
14 J. Li, S. Kamin, G. Zheng, F. Neubrech, S. Zhang and N. Liu, *Sci. Adv.*, 2018, **4**, eaar6768.
15 Q. Zhou, X. Dong, Y. Xiong, B. Zhang, S. Lu, Q. Wang, Y. Liao, Y. Yang and H. Wang, *ACS Appl. Mater. Interfaces*, 2020, **12**, 28539–28549.
16 H. Sun, S. Liu, W. Lin, K. Y. Zhang, W. Lv, X. Huang, F. Huo, H. Yang, G. Jenkins and Q. Zhao, *Nat. Commun.*, 2014, **5**, 3601.
17 Z. Sun, J. Yang, L. Huai, W. Wang, Z. Ma, J. Sang, J. Zhang, H. Li, Z. Ci and Y. Wang, *ACS Appl. Mater. Interfaces*, 2018, **10**, 21451–21457.
18 P. Shi, Y. Li, Z. Xu, Y. Duan, Y. Liu, R. Zhao, M. Zhang and T. Han, *Dyes Pigm.*, 2019, **162**, 272–280.

19 X. Li, Y. Xie, B. Song, H. L. Zhang, H. Chen, H. Cai, W. Liu and Y. Tang, *Angew. Chem., Int. Ed.*, 2017, **56**, 2689–2693.
20 Z. Tian, D. Li, E. V. Ushakova, V. G. Maslov, D. Zhou, P. Jing, D. Shen, S. Qu and A. L. Rogach, *Adv. Sci.*, 2018, **5**, 1800795.
21 Q. Zhu, K. Van Vliet, N. Holten-Andersen and A. Miserez, *Adv. Funct. Mater.*, 2019, **29**, 1808191.
22 Z. Li, H. Chen, B. Li, Y. Xie, X. Gong, X. Liu, H. Li and Y. Zhao, *Adv. Sci.*, 2019, **6**, 1901529.
23 Y. Cheng, K. Ren, D. Yang and J. Wei, *Sens. Actuators, B*, 2018, **255**, 3117–3126.
24 A. H. Milani, J. M. Saunders, N. T. Nguyen, L. P. Ratcliffe, D. J. Adlam, A. J. Freemont, J. A. Hoyland, S. P. Armes and B. R. Saunders, *Soft Matter*, 2017, **13**, 1554–1560.
25 Y. Zhang, J. Liao, T. Wang, W. Sun and Z. Tong, *Adv. Funct. Mater.*, 2018, **28**, 1707245.
26 X. Le, W. Lu, H. Xiao, L. Wang, C. Ma, J. Zhang, Y. Huang and T. Chen, *ACS Appl. Mater. Interfaces*, 2017, **9**, 9038–9044.
27 E. O. Akala, P. Kopečková and J. Kopeček, *Biomaterials*, 1998, **19**, 1037–1047.
28 I.-S. Kim, S.-H. Kim and C.-S. Cho, *Arch. Pharmacal Res.*, 1996, **19**, 18–22.
29 H. Wen, S. Song, F. Xie, B. Wang, J. Xu, Z. Feng, S. Wu, J. Han, B.-O. Guan and X. Xu, *Mater. Horiz.*, 2020, **7**, 3201–3208.
30 W. Li, J. Xu, Q. Zhou, S. Wang, Z. Feng, D. Hu, X. Li and Y. Cao, *Nanoscale*, 2018, **10**, 21910–21917.
31 E. Kokufuta, B. Wang, R. Yoshida, A. R. Khokhlov and M. Hirata, *Macromolecules*, 1998, **31**, 6878–6884.
32 Y. Y. Cao, N. Takeyasu, T. Tanaka, X. M. Duan and S. Kawata, *Small*, 2009, **5**, 1144–1148.
33 L. V. Wang and S. Hu, *Science*, 2012, **335**, 1458–1462.